THE JOURNAL OF PHYSICAL CHEMISTRY C

Article

Cite This: J. Phys. Chem. C 2019, 123, 23410−23418

pubs.acs.org/JPCC

Dissolution of $BiVO_4$ Photoanodes Revealed by Time-Resolved Measurements under Photoelectrochemical Conditions

Siyuan Zhang,*[,†] Martin Rohloff,[‡,§,∥] Olga Kasian,[†,⊥] Andrea M. Mingers,[†] Karl J. J. Mayrhofer,[†,#,%] Anna Fischer,[‡,§,∥] Christina Scheu,[†] and Serhiy Cherevko*[,#]

[†]Max-Planck-Institut für Eisenforschung GmbH, Max-Planck-Straße 1, 40237 Düsseldorf, Germany

[‡]Freiburger Zentrum für interaktive Werkstoffe und bioinspirierte Technologien, Albert-Ludwigs-Universität Freiburg, Georges-Köhler-Allee 105, 79110 Freiburg, Germany

[§]Institut für Anorganische und Analytische Chemie, Albert-Ludwigs-Universität Freiburg, Albertstraße 21, 79104 Freiburg, Germany

[∥]Freiburger Materialforschungszentrum, Stefan-Meier-Straße 19, 79104 Freiburg, Germany

[⊥]Helmholtz-Zentrum Berlin, Helmholtz-Institute Erlangen-Nürnberg, 14109 Berlin, Germany

[#]Helmholtz-Institute Erlangen-Nürnberg for Renewable Energy (IEK-11), Forschungszentrum Jülich, 91058 Erlangen, Germany

[%]Department of Chemical and Biological Engineering, Friedrich-Alexander-Universität Erlangen-Nürnberg, Egerlandstr. 3, 91058 Erlangen, Germany

ABSTRACT: Photocorrosion imposes a fundamental limit to the longevity of devices that harvest energy from photons. As one of the best performing electrode materials for photoelectrochemical water oxidation reaction, $BiVO_4$ undergoes photocorrosion with various postulated mechanisms under debate. We present time-resolved dissolution measurements to advance the mechanistic understanding, enabled by the recent development in illuminated scanning flow cell coupled to inductively coupled plasma mass spectrometry. The contact dissolution of predominantly V was distinguished from the stoichiometric photoelectrochemical dissolution of Bi and V. The citrate electrolyte was utilized to form soluble complexes with dissolved Bi and to act as hole scavengers that provide photocurrents at a wide range of potentials. The photoelectrochemical dissolution rates remain similar between 0.4 and 1.6 V vs reversible hydrogen electrode and become lower at the open circuit potential, 0.2 V. The time-resolved measurements support oxidation of Bi(III) by photogenerated holes as the main mechanism for photocorrosion.

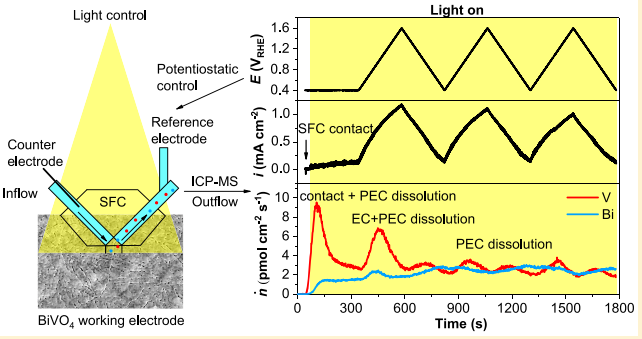

INTRODUCTION

Photoelectrochemical (PEC) water splitting transforms sunlight, the most abundant renewable energy source, into H_2, the ideal fuel for a carbon-free economy. To integrate the mature photovoltaic and water electrolysis technologies into single PEC water splitting devices, the stability of photoelectrodes in the aqueous environment remains a big challenge.[1] Indeed, in recent years, there has been ongoing research and development of materials that generate sufficient photovoltage under sunlight, while their stability under PEC conditions is still to be proven. One of the most studied photoabsorbers is bismuth vanadate, $BiVO_4$.

$BiVO_4$ has been studied for photocatalytic[2] and PEC[3] oxidation of water. The monoclinic phase shows the highest photocatalytic activity and has a band gap of 2.4 eV.[4] It has been established as one of the best performing photoanode materials for the water oxidation reaction.[5−10] $BiVO_4$ has low conductivity, and the charge carriers are prone to recombination. These can be respectively mitigated by doping of e.g. W, Mo,[11] or F[12] and heterojunction band engineering with e.g. WO_3 or SnO_2.[6] Another bottleneck, the sluggish reaction of holes with water, can be optimized by applying water oxidation catalysts on the surface of the $BiVO_4$ absorber.[5,9] Today, $BiVO_4$ photoanodes can reach current densities close to the theoretical limit of 7.5 mA cm^{-2}.[10,13] It has been demonstrated that a lower band gap absorber, Fe_2O_3, can be used in tandem to extend the limit.[14]

Despite the ongoing development of $BiVO_4$ photoanodes, their stability remains puzzling with seemingly contradicting phenomena reported and various postulated corrosion mechanisms under debate. The drop in $BiVO_4$ photocurrent under potential hold has been first reported by Sayama et al.,[15] where they also found that a surface treatment by $AgNO_3$ both enhanced the photocurrent and slowed down its decay. Berglund et al.[16] used inductively coupled plasma mass spectrometry (ICP-MS) to quantify the dissolution of $BiVO_4$

Received: July 29, 2019
Revised: August 23, 2019
Published: September 3, 2019

into electrolyte after PEC operation (*ex situ*). They have characterized V dissolution from the $BiVO_4$ film with excess amount of V but did not find dissolution from the stoichiometric $BiVO_4$ film. $BiVO_4$ was hence considered stable against photocorrosion.[16] Two recent studies have demonstrated the dissolution of $BiVO_4$ in neutral and alkaline media by *ex situ* ICP-MS or ICP-optical emission spectrometry (OES). Toma et al.[17] have found a continuous decrease in $BiVO_4$ layer thickness under operation by means of electron microscopy and scanning probe microscopy, resulting in the stoichiometric dissolution of Bi and V. In contrast, Lee and Choi[18] have found that V dissolves much more than Bi from the electrode. They have demonstrated inhibition of the dissolution by using an electrolyte saturated with V(V)[a] and over 500 h stability operating at 0.6 V_{RHE}[b] and over 3 mA cm^{-2}.

Chen and Wang studied possible corrosion reactions for many photoelectrodes at pH = 0.[19] However, their identified corrosion reaction, $4BiVO_4 + 12H^+ + 12Cl^- \rightarrow 4BiCl_3 + 2V_2O_5 + 6H_2 + 3O_2$, at the equilibrium potential 1.24 V_{RHE}, involves Cl^- ions in the aqueous media. Nevertheless, they reach the conclusion that $BiVO_4$ is stable, as the corrosion reaction has a more positive potential than the oxygen evolution reaction (OER). On the other hand, $BiVO_4$ is unstable with respect to the OER according to the Pourbaix diagram calculated in ref 17. At potentials cathodic to OER, the BiO^+ ion or Bi_4O_7 solid is found stable together with the $[VO_4]^-$ ion. It is nevertheless suggested that the Bi_4O_7 phase may act as a passivation layer.

To identify the mechanism of $BiVO_4$ photocorrosion, parameters such as light and the operating potential need to be controlled independently. Time-resolved dissolution measurements enable studying these effects in operando on the same sample. This has been developed on a scanning flow cell (SFC) coupled to ICP-MS to ensure the time resolution and enhance the detection sensitivity.[20,21] The SFC-ICP-MS setup has been applied to study the corrosion of metals, coatings, and catalysts. Recently, it has been adapted to study photocorrosion of WO_3 by introducing light control into the SFC-ICP-MS setup.[22]

The direct integration with ICP-MS imposes an upper limit on the ionic strength of the electrolyte to a few tens of mM. In this study, we chose the chelating electrolyte sodium citrate buffered at neutral pH. Citrate is a good chelating reagent, which can keep dissolved Bi and V ions in the aqueous solution to reach the detector of the ICP-MS for quantification. In this way, the intrinsic stability and photostability of $BiVO_4$ can be examined. Furthermore, citrate oxidation is thermodynamically more favorable with respect to water oxidation. Using citrate as the hole scavenger enables shifting the photocurrent onset of photoanodes toward lower potentials,[23] and hence we can compare the activity and corrosion of $BiVO_4$ in a wide potential range without introducing electrocatalysts.

The time resolution is demonstrated pivotal in this study to differentiate the contact and electrochemical (EC) dissolution from the following near-stoichiometric PEC dissolution. With the new insights gained from time-resolved measurements, we critically review different corrosion and photocorrosion mechanisms of $BiVO_4$ and reconcile some seemingly contradicting observations from the literature.

EXPERIMENTAL SECTION

The synthesis of $BiVO_4$ has been reported by Rohloff et al.[11] Bismuth 2-ethylhexanoate and vanadium oxytriethoxide were mixed and stirred for 4 h to form a homogeneous precursor solution. Then, the solution was dip-coated on fluorine-doped tin oxide substrates, which were then calcined at 450 °C for 2 h.

The PEC experiments were performed in a micro-electrochemical SFC[20,21] using a Gamry Reference 600 potentiostat. The geometric sample area that served as working electrode was about 0.01 cm^2. The counter electrode (Pt wire, 0.5 mm, 99.997%, Alfa Aesar) was placed in the inlet channel and the reference electrode (Ag/AgCl/3 M KCl, 1 M = 1 mol dm^{-3}) in the outlet channel of the SFC. The 5 and 15 mM citrate buffer solutions were prepared from citric acid monohydrate (p.A. Merck) and 4 M sodium hydroxide solution (Titrisol, Merck) in a molar ratio of 0.34:1. The pH values were measured by the pH meter WTW MultiLab 540 and determined to be between 6.95 and 7.05. Front illumination was introduced by a light source (Lumatec Superlite) filtered to the 400−700 nm spectral range. Guided through a liquid light guide and collimating lenses, the intensity at the working electrode was calibrated to be 100 mW cm^{-2} by using a Si-diode photometer (Newport).

The electrolyte was pumped with a flow rate of 3.4 μL s^{-1} through the cell and subsequently introduced into the ICP-MS (NexION 300X, PerkinElmer) for time-resolved analysis of the amount of dissolved ions of vanadium and bismuth (^{51}V and ^{209}Bi isotopes were measured). The detected intensities were analyzed with respect to an internal standard for compensation of physical interferences. ^{89}Y was used for V and ^{187}Re for Bi. Both elements were added to the electrolyte via a Y-shaped connector in a solution of 0.5% HNO_3 (65%, Suprapur, Merck) behind the SFC. ICP-MS calibration was performed on a daily basis prior to the measurements and used to convert the detected intensities to the concentration of the dissolved ions in the electrolyte.

An anodic photocurrent of 1 mA cm^{-2} from the 0.01 cm^2 cell corresponds to consuming 0.1 nmol s^{-1} of photogenerated holes and releasing as much H^+ ($2H_2O + 4h^+ = O_2 + 4H^+$). By considering the flow rate of 3.4 μL s^{-1}, a 31 μM concentration of H^+, or pH = 4.5, would be reached in the absence of buffers. One millimole of citrate buffer has a capacity to buffer 0.3 mmol of H^+, reducing the pH from 7 to 6. Therefore, for our lowest concentration of citrate buffer at 5 mM, 1.5 mM H^+ can be buffered until pH = 6. Assuming linearity of the buffer capacity, 31 μM H^+, corresponding to a photocurrent of 1 mA cm^{-2} in our SFC setup, is only expected to cause a drop of pH from 7 to 6.98.

Scanning electron microscopy (SEM) micrographs were taken by using a Thermo Fischer Scios2 microscope operated at 30 kV. Energy dispersive X-ray spectroscopy (EDS) spectra were recorded at the same SEM operation conditions by a EDAX spectrometer and quantified by the software.

X-ray photoelectron spectra (XPS) were measured (Quantera II, Physical Electronics, Chanhassen, MN) using a monochromatic Al Kα X-ray source (1486.6 eV) and operating at 15 kV and 25 W. The binding energy scale was referenced to the C 1s signal at 285.0 eV. The Casa XPS software was used to analyze the experimentally obtained spectra.

DOI: 10.1021/acs.jpcc.9b07220
J. Phys. Chem. C 2019, 123, 23410−23418

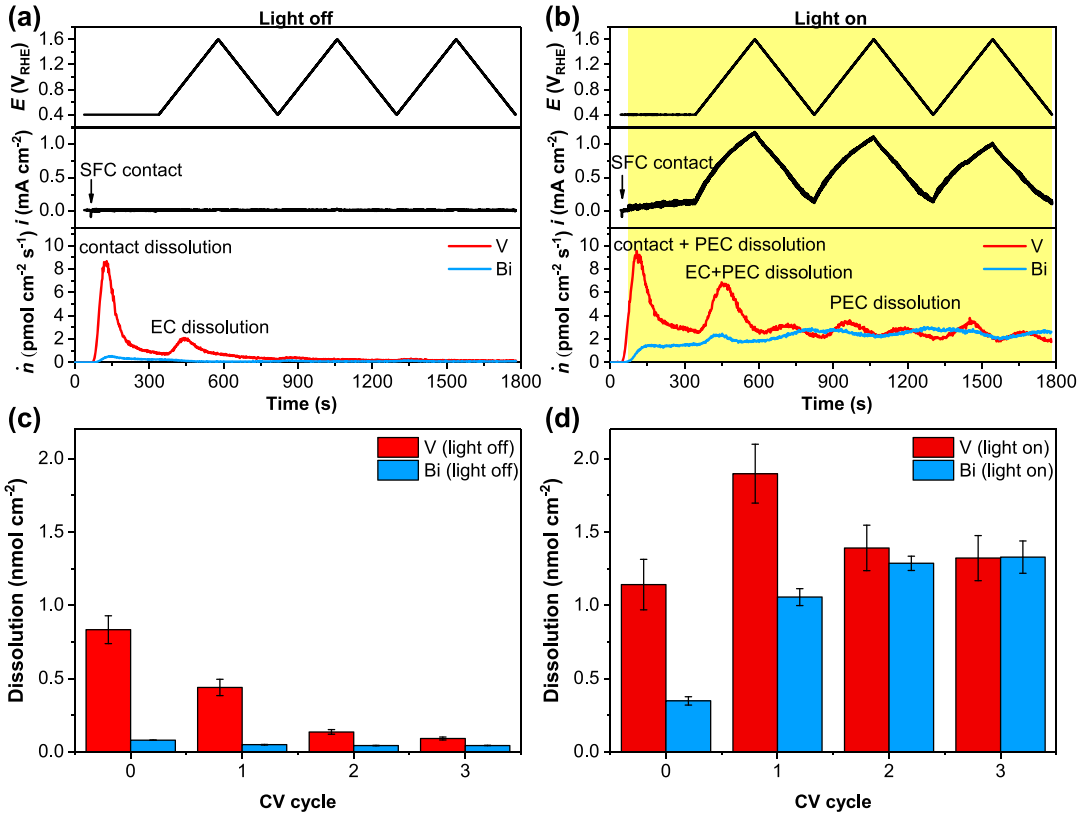

Figure 1. Time profiles of applied potential to the $BiVO_4$ photoanode, current density (i), and dissolution rates ($\dot{n}$) of Bi and V during (a) light-off and (b) light-on CV scans in the 15 mM citrate buffer and integrated amount of dissolution at contact and different CV cycles of $BiVO_4$ during (c) light-off and (d) light-on scans. Error bars are standard deviation from measurements on multiple spots.

RESULTS

We use $BiVO_4$ thin film photoanodes synthesized by a scalable chemical route reported in our previous study.[11,12] The porous $BiVO_4$ films are ~270 nm in thickness and have pore sizes of several tens of nanometers. On the micrometer scale, they homogeneously cover the fluorine-doped tin oxide substrate and have a specific surface area ~8 times the geometrical area.[11] Without any doping or surface modification, a photocurrent of 0.2 mA cm^{-2} at 1.23 V_{RHE} was achieved under an illumination of 100 mW cm^{-2} (white light, 400−700 nm). Although by introducing water oxidation catalysts a photocurrent of over 2 mA cm^{-2} at 1.23 V_{RHE} was demonstrated,[11] it is not discussed in this mechanistic study because electrocatalysts partially block the interface between $BiVO_4$ thin film and the electrolyte.

Time Resolution and Cyclic Voltammetry. First, we exemplify the time- and potential-resolution capacity of the in operando measurements. A scheme of the SFC-ICP-MS setup is presented in ref 22. Unlike in ref 22, a broad-band light source filtered to 400−700 nm was introduced as front illumination in this work instead of a single-wavelength light-emitting diode. The $BiVO_4$ working electrodes were set at 0.4 V_{RHE} while approached by the SFC. As a visual guide is needed, the SFC contact was only established in the dark, i.e., without intensive illumination. As marked by the arrows in Figures 1a and 1b, a contact current was measured once the working electrode is connected to the SFC. With regard to the ICP-MS data, as soon as the contact was established between the working electrode and the SFC, dissolution of Bi and V was observed that peaks in the following minutes. The contact dissolution of V is more intense than that of Bi.

The potential was held at 0.4 V_{RHE} for 5 min to allow the contact dissolution peaks to tail off. Subsequently, three cyclic voltammetry (CV) scans between 0.4 and 1.6 V_{RHE} were introduced to investigate the effect of potential on the $BiVO_4$ dissolution. This potential protocol was performed either in the dark (Figure 1a) or under light at a constant flux of 100 mW cm^{-2} (Figure 1b). For the light-on measurements, the illumination was from the front side (the interface between electrolyte and $BiVO_4$) of the working electrode and switched on during the potential hold at 0.4 V_{RHE}, as highlighted by the colored region in Figure 1b. During the light-off protocol, negligible Faradaic current was observed on the $BiVO_4$ electrode between 0.4 and 1.6 V_{RHE}. A gradual increase of the photocurrent with the potential, reaching a current density of ~1 mA cm^{-2} at 1.6 V_{RHE} (Figure 1b), was obtained during the light-on protocol.

The integrated amount of dissolved V and Bi during each CV cycle is summarized in Figures 1c and 1d. Measurements of identical PEC protocols from different sample areas show good reproducibility. The dissolution rates are integrated over the time spans of the contact and subsequent CV cycles, where the error bars indicate the spread of measurements on different areas. Before the first CV cycle (labeled as 0 in Figures 1c and 1d), the dissolution was caused by the contact and potential hold at 0.4 V_{RHE}. Higher amounts of dissolution during the zeroth phase under light are attributed to PEC dissolution in addition to contact dissolution. Dissolution under light is higher during the first cycle and levels off from the second CV cycle onward. In comparison, dissolution tails toward less than

DOI: 10.1021/acs.jpcc.9b07220
J. Phys. Chem. C 2019, 123, 23410−23418

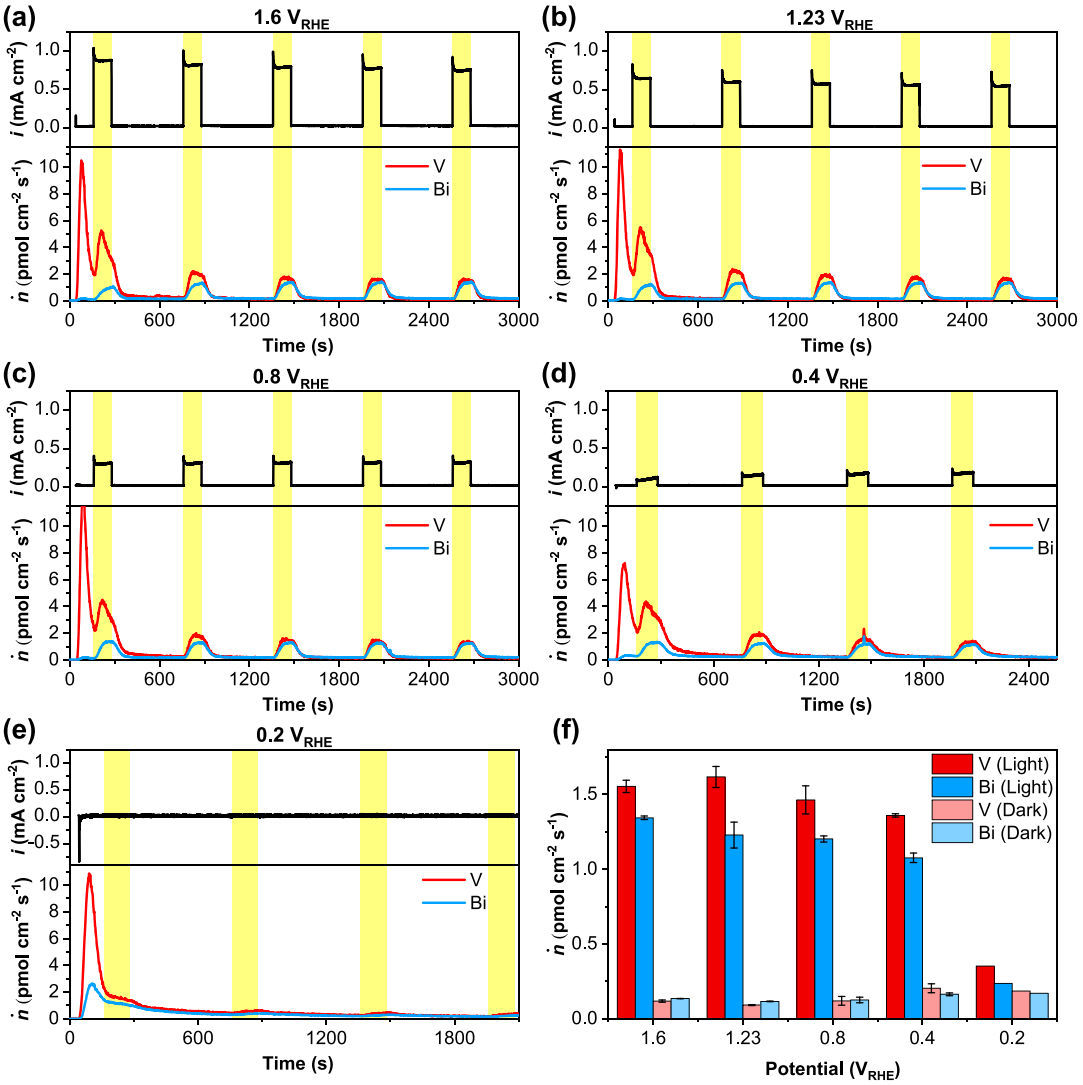

Figure 2. Dissolution of Bi and V from $BiVO_4$ at (a) 1.6, (b) 1.23, (c) 0.8, (d) 0.4, and (e) 0.2 V_{RHE} in the 15 mM citrate buffer and (f) summary of the PEC dissolution rates and the EC dissolution rates in the dark. Error bars are standard deviation from measurements on multiple spots.

0.1 nmol cm^{-2} in the dark, an order of magnitude smaller than the dissolution under light. Therefore, PEC corrosion is accountable for most of the dissolution under light observed from the second CV cycle onward.

Nevertheless, an appreciable amount of V dissolution was observed in the dark during the anodic sweep of the first CV scan (Figure 1a). This peak is assigned as EC dissolution to differentiate it from the PEC dissolution where light is the determining factor. The integrated amount of the EC dissolution of V, ~0.5 nmol cm^{-2}, is similar to the difference between the V dissolution under light measured during the first CV cycle and the PEC dissolution of each of the subsequent cycles (Figure 1b). Therefore, the corresponding peak in Figure 1b was assigned to be a combination of EC and PEC dissolution.

The time resolution of in operando measurements opens up design space of PEC protocols to separate contact, EC, and PEC dissolution. For the PEC protocols above, the contact dissolution and EC dissolution diminish with time. During these stages, the dissolution is clearly off stoichiometric, with a much higher content of V than Bi. In contrast, PEC dissolution was repeated among the CV cycles in trends and magnitude. Moreover, Bi and V dissolve at similar molar rates that fluctuate mildly with the potential between 2 and 3 pmol cm^{-2} s^{-1}. V dissolution peaks at ~1 V_{RHE}, whereas Bi dissolution peaks at ~0.6 V_{RHE} for both anodic and cathodic scans.

Chronoamperometry. As the next step, we designed chronoamperometry measurements to study the operation of photoanodes under fixed potentials. For the mechanistic understanding of corrosion, holding potentials at 1.6, 1.23, 0.8, 0.4, and 0.2 V_{RHE} were studied, as shown in Figure 2. The range spans from over the OER potential down until the open circuit potential of $BiVO_4$ under light, 0.2 V_{RHE}. It is apparent from the time-resolved measurements in Figure 2 that the contact dissolution can be distinguished from the subsequent PEC dissolution.

Like the CV experiments in Figure 1, contact to the SFC was established in the dark. The measured current upon contact decreases as the holding potential decreases. At 1.6 and 1.23 V_{RHE}, the contact current is anodic. At 0.8 V_{RHE}, the contact current is close to 0. At 0.4 and 0.2 V_{RHE}, a cathodic contact current is observed. On the other hand, the contact dissolution at all five potentials is very similar, ~1 nmol cm^{-2} of integrated

DOI: 10.1021/acs.jpcc.9b07220
J. Phys. Chem. C 2019, 123, 23410−23418

V dissolution and 0−0.2 nmol cm^{-2} of Bi dissolution (see Figure 1c for the contact at 0.4 V_{RHE}).

To study the effect of illumination, light-on (2 min) and light-off (8 min) cycles were introduced during the chronoamperometry measurements, as highlighted by the light on windows in Figure 2. At the first instance of light on, there is still a higher amount of V dissolution than Bi dissolution. In the subsequent light on windows, the dissolution of V and Bi becomes closer to the 1:1 stoichiometry of $BiVO_4$. As the light is switched on, Bi and V dissolution rates sharply increase until a plateau is reached, from which the PEC dissolution rates are evaluated. As the light is switched off, Bi and V dissolution rates decrease exponentially toward the EC dissolution rates in the dark. A comparatively longer light off time of 8 min was chosen to allow the PEC dissolution to tail off.

To test the dependence of PEC dissolution rates on the concentration of citrate electrolyte, $BiVO_4$ photoanodes were also tested in the 5 mM citrate buffer solution, as shown in Figure 3a. Instead of a constant potential hold, four potentials are staggered in the protocol with light-on/off windows in between.

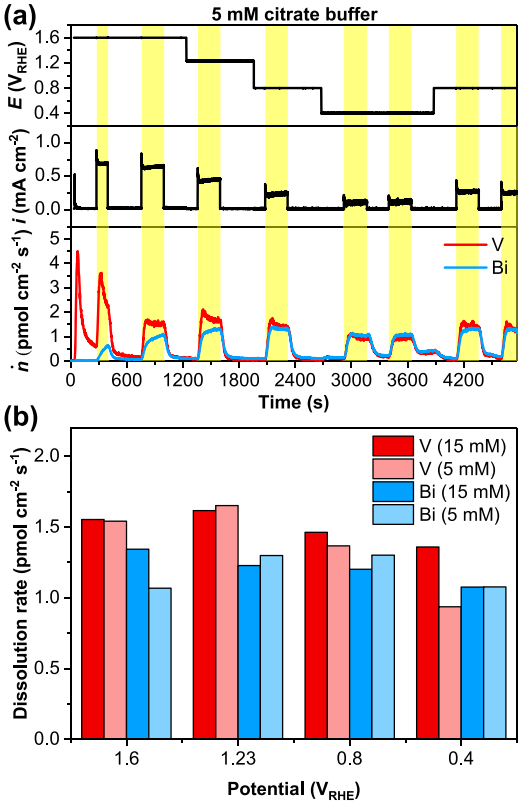

Figure 3. (a) Dissolution of Bi and V from $BiVO_4$ at various holding potentials in the 5 mM citrate buffer. (b) Comparison between PEC dissolution rates in the 15 and 5 mM citrate buffer.

From the second light-on/off cycles onward (Figure 2), the PEC and EC dissolution rates, determined at the end of the respective light-on and -off windows, are very well reproduced. As summarized in Figure 2f, the dissolution of Bi and V is close to stoichiometry both under and without illumination. Moreover, as shown in Figure 3b, the PEC dissolution rates determined in the 15 and 5 mM citrate buffer are very similar. For the measurement protocol in the 5 mM citrate buffer (Figure 3a), however, the EC dissolution rates in the dark may not be accurately evaluated due to a shorter light off time and more frequent changes in the holding potentials.

At 0.2 V_{RHE}, a mild increase of dissolution is observed during illumination despite having negligible photocurrent. At all other four potentials where a photocurrent is clearly measured, there is an order of magnitude contrast between the PEC dissolution rates, 1.3−1.6 pmol cm^{-2} s^{-1} for V (1.1−1.3 pmol cm^{-2} s^{-1} for Bi) and those in the dark, 0.1−0.2 pmol cm^{-2} s^{-1}. Moreover, between 0.4 and 1.6 V_{RHE}, the PEC dissolution rates are constant within the statistical scatters from the measurements (Figure 2f), and so are the EC dissolution rates in the dark. The lack of dependence of PEC dissolution on the holding potential in this range corresponds well to the slowly varying dissolution rates in the CV scans (Figure 1b). It is, however, noticeable that the PEC dissolution rates measured during steady potential hold are only about half as much as those measured at dynamic conditions during the CV scans.

Correlation with Surface Composition. The microstructure of the porous $BiVO_4$ film before and after the PEC protocols was examined by SEM. As shown in Figure 4, the SFC contact area is conveniently identified by the dried citrate electrolyte left on top. The comparison between the areas within the SFC (after PEC, Figure 4d) and without (as synthesized, Figure 4c) shows hardly any changes in their morphology. As shown in Table 1, EDS analysis on Bi and V does not indicate a compositional change throughout the thickness of the film. A change in the chemical composition was observed by XPS measurements, as the surface becomes slightly Bi-enriched after the PEC protocol.

DISCUSSION

The time resolution offered by in operando dissolution measurements helps unveil complicated phenomena of $BiVO_4$ dissolution under PEC conditions. Contact, EC, and PEC dissolution can be identified by their respective dependence on time, the applied potential, and illumination. These dissolution processes likely involve different mechanisms, and it is very beneficial to investigate them separately.

Contact Dissolution. As shown in Figure 1, about 1 nmol cm^{-2} V is dissolved upon contact, which is a major contribution to the total amount of dissolution in the dark (Figure 1c). As 1 mol $BiVO_4$ has 323.92 g of mass and 53.1 cm^3 of volume, 1 nmol cm^{-2} translates to removal of V from ∼0.5 nm of a compact $BiVO_4$ layer. To dissolve 1 nmol cm^{-2} of $BiVO_4$ at the PEC dissolution rates of 1.1−1.6 pmol cm^{-2} s^{-1} under 100 mW cm^{-2} illumination and 0.1−0.2 pmol cm^{-2} s^{-1} in the dark would take 10−15 and 80−170 min, respectively. For an integrated dissolution measurements after 1 h of PEC operation, contact dissolution would still be the major contribution in the dark and account for 15−20% of the measured dissolution under light. Therefore, separation of contact dissolution by time-resolved measurements is especially crucial to evaluate the lower dissolution rates in the dark.

The integrated dissolution measurements from the literature do not offer much discussion on contact dissolution. It is suggested by Lee and Choi[18] that most V dissolution from V-excess films of Berglund[16] may have happened upon contact by the dissolution of V-rich oxides (such as V_2O_5) on the $BiVO_4$ surface. To exclude contact dissolution, Lee and Choi applied chemical treatment prior to PEC measurements to standardize the surfaces under investigation.[18] By following their procedure

DOI: 10.1021/acs.jpcc.9b07220
J. Phys. Chem. C 2019, 123, 23410−23418

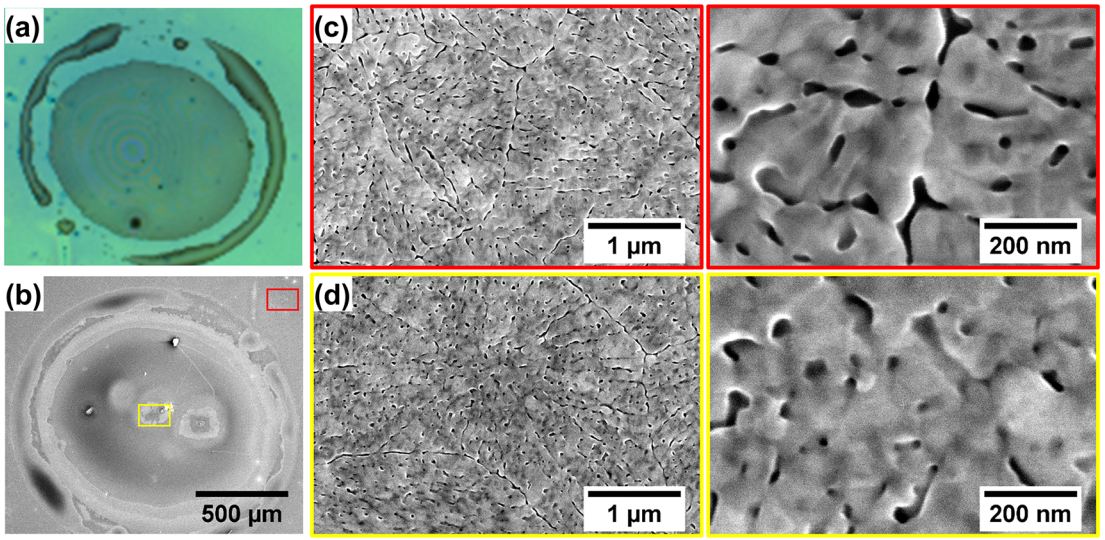

Figure 4. Top view of the SFC contact area on the $BiVO_4$ surface by (a) optical micrograph and (b, c, d) SEM micrographs at different magnifications showing the surface morphology from (c) as-synthesized areas and (d) those after the PEC protocol from Figure 2d.

Table 1. Stoichiometry of $BiVO_4$ Surface and Bulk before and after the PEC Protocol

V/Bi (mol %)	surface composition (XPS)	bulk composition (EDS)
as synthesized	51.2/48.8	50.7/49.3
after PEC	46.0/54.0	50.4/49.6

immersing our $BiVO_4$ films into 1 M NaOH for 15 min, however, a contact dissolution peak of primarily Bi instead of V was observed. Their strategy to reduce contact dissolution does not apply here, which may be due to the difference in the synthesis of $BiVO_4$ films. A separate time-resolved study will aid the search for means to minimize contact dissolution, which is however beyond the scope of this work.

As shown in Figure 2, there is a similar amount of dissolution of V and Bi during contact, whether the contact current is anodic or cathodic. At ~0.8 V_{RHE}, similar contact dissolution is observed at a negligibly small contact current. As charges can flow in either direction depending on the potential, it is unlikely that the contact dissolution is caused by one particular redox reaction. Hence, a charge-neutral reaction is likely responsible for the contact dissolution.

V_2O_5 is known to dissolve in aqueous solutions.[15] In the V–H_2O Pourbaix diagram,[24,25] V_2O_5 is only predicted stable at low pH < 3 and high V(V) concentrations. At around neutral pH, ions such as $H_2VO_4^-$ and $V_4O_{12}^{4-}$ exist in the aqueous phase, depending on the V(V) concentration.[25] V(V) may also form complexed ions with citrate.[26] To simplify the mechanistic picture, all dissolved V(V) species are generalized as $V(V)_{aq}$, as shown by reaction 3 in Scheme 1.

No charge transfer is involved in reaction 3, as the contact dissolution at different potentials remains similar regardless of the varying contact currents. The reaction readily proceeds to dissolve any excess of V_2O_5 on the surface of $BiVO_4$. There is also the possibility of contact dissolution of V from stoichiometric $BiVO_4$, leaving a Bi-rich surface as suggested by the post-PEC compositional analysis (Table 1). The Bi-rich surface of $BiVO_4$ has also been reported in the literature, which becomes more Bi-rich after PEC degradation.[1]

PEC Dissolution: Resolving the Discrepancy in the Literature. The dissolution stability of $BiVO_4$ has been

Scheme 1. Possible Reactions of $BiVO_4$ Photoanodes in the Discussion[a]

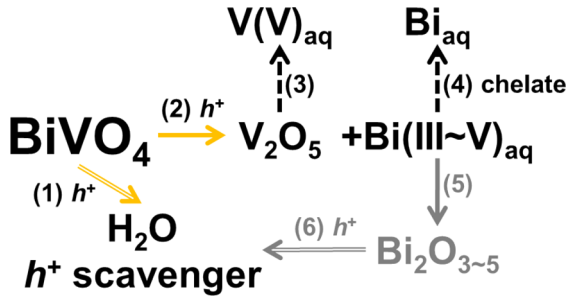

[a]The oxidation reactions involving photogenerated holes [(1) and (2)] are colored in yellow. The transfer of holes in (1) and (6) are marked by hollow-line arrows. The dissolution reactions (3) and (4) are marked by dashed lines, and the possible precipitation reaction (5) is marked by a gray solid line.

quantitatively evaluated by ICP-MS[16,17] or ICP-OES[18] in several experimental studies. It is worth noting that all previous reports are *ex situ* integrated measurements without time resolution and hence unable to differentiate PEC dissolution from the contact dissolution. Berglund et al. measured stoichiometric $BiVO_4$ tested in 0.1 M Na_2SO_4 electrolyte (not buffered in pH) and found neither V nor Bi in the electrolyte.[16] However, their electrolytes were heavily diluted by 1:100 or 1:1000 before the ICP-MS measurements, which means that the concentrations of dissolved Bi and V ions may have fallen below their respective detection limits. In a more recent report, Lee and Choi measured in 1 M $K_2B_4O_7$ electrolyte (pH 9.3) and diluted only by 1:2 before the ICP-OES analysis. They have clearly observed a significant amount of dissolved V and a lower amount of dissolved Bi.[18] Finally, Toma et al. measured in phosphate buffers (K_2HPO_4 at pH = 6.8 or K_3PO_4 at pH = 12.3) at 0.1 or 1 M and observed close to stoichiometric Bi and V dissolution.[17] The major discrepancy between the last two reports is the amount of Bi dissolution with respect to V dissolution.

According to the Bi–H_2O Pourbaix diagram,[27] Bi(III) and Bi(V) oxides are insoluble in water at neutral and alkaline pH.

DOI: 10.1021/acs.jpcc.9b07220
J. Phys. Chem. C 2019, 123, 23410–23418

Therefore, suppose $BiVO_4$ did dissolve, Bi ions would not be stable in water and would form insoluble compounds, as described by reaction 5 in Scheme 1. It is also worth noting that Bi(V) can oxidize water and return to Bi(III),[27] as indicated by reaction 6.

With the presence of a chelating reagent, such as the citrate electrolyte used in this study, dissolved Bi can form complex ions and remain in the aqueous phase, described by the general notation Bi_{aq} in reaction 4 of Scheme 1. Bi(III) citrate complexes have been studied in pharmacology.[28,29] Their water solubility has been determined to be over 10 mg L^{-1} at 20 °C,[30] i.e., 25 μM of Bi. Saturated Bi(III) citrate flowing through SFC of 0.01 cm^2 at 3.4 $\mu L\ s^{-1}$ would be measured at 8 nmol $cm^{-2}\ s^{-1}$, 3−4 orders of magnitude higher than measured dissolution rates in Figures 1−3. In addition, Bi(III) citrate is known to solubilize by NH_4OH and KOH, forming complex ions[28] with the units $[Bi_2cit_2(H_2O)_2]^{2-}$, which are the likely species entering the ICP-MS for the quantification of Bi_{aq}.

As V(V) is soluble in water, a chelating reagent to keep dissolved Bi ions in the electrolyte would preserve the 1:1 stoichiometric dissolution of V and Bi from $BiVO_4$. We have demonstrated that the 5 mM citrate buffer is sufficient to chelate dissolved Bi ions, as the dissolution rates remain very similar compared to those measured in the 15 mM citrate buffer (Figure 3b). Our observation of stoichiometric PEC dissolution agrees with the results measured in phosphate buffers.[17] Pyrophosphate and triphosphate are known for chelating ions.[31] The concentration of these polymeric phosphate ions would increase with increasing phosphate concentration, which may explain the higher Bi dissolution measured in the 1 M than in the 0.1 M phosphate buffer.[17]

As a chelating reagent could favor the dissolution of $BiVO_4$, it is useful to compare our measured dissolution rates in neutral 5 and 15 mM citrate buffers with available reports in the literature, measured in 0.1 and 1 M phosphate buffers.[17] Note that the dissolution rates from ref 17 were derived from integrated measurements assuming a constant dissolution rate. To convert our unit pmol $cm^{-2}\ s^{-1}$ to nm min^{-1}, a multiplication factor of 0.032 is applied for $BiVO_4$. The respective dissolution rates of 0.023 and 0.126 nm min^{-1} in 0.1 and 1 M phosphate buffers at pH 6.8, 1.23 V_{RHE} and 100 mW cm^{-2} illumination[17] envelope our measured rates of ∼0.05 nm min^{-1} (1.5 pmol $cm^{-2}\ s^{-1}$). For their measurements in the dark in 1 M phosphate buffer at pH 6.8, 1.23 V_{RHE}, the rate 0.049 nm min^{-1} is an order of magnitude higher than our measurement of ∼0.005 nm min^{-1} (0.15 pmol $cm^{-2}\ s^{-1}$). As mentioned above, time-resolved measurements can benefit from the determination of lower dissolution rates by excluding the contribution from contact dissolution.

PEC Dissolution: Possible Mechanisms. Unlike contact dissolution, PEC dissolution must involve a redox reaction. The clear order of magnitude difference between the light-on and light-off dissolution rates suggests the important role of photogenerated holes. Lee and Choi[18] proposed selective leech-out of V as the main mechanism of $BiVO_4$ photocorrosion. In the $BiVO_4$−H_2O Pourbaix diagram,[17] V(VII) species such as VO_4^- are suggested. However, further oxidation of V(V), which would require removal of the inner shell 3s/3p electrons from V, has not been reported in the V−H_2O Pourbaix diagrams.[24,25]

The oxidation of Bi(III) has also been proposed as a possible mechanism for the PEC dissolution.[1] In the calculated $BiVO_4$−H_2O Pourbaix diagram,[17] Bi_4O_7 solid exists with a mixed oxidation states of Bi(III) and Bi(V). Similarly, the Bi−H_2O Pourbaix diagram[27] contains the insoluble Bi_4O_7, Bi_2O_4, and Bi_2O_5. The apparent difficulty for this interpretation is the formation of insoluble Bi phases. It was attempted to remove the Bi_4O_7 phase from the $BiVO_4$−H_2O Pourbaix diagram,[17] resulting in Bi(III) species such as BiO^+ at neutral pH. However, as discussed in the previous section, the presence of chelating reagents can be responsible for the Bi detection from the electrolyte.

We therefore propose oxidation of Bi(III) as the main mechanism for $BiVO_4$ dissolution. In Scheme 1, reaction 2 describes the primary process where the photogenerated holes oxidize Bi(III) in $BiVO_4$, causing the release of Bi ions into the electrolyte. The reaction can proceed as long as holes are available on the surface, as any V(V) species (e.g., V_2O_5) left after the Bi dissolution would be dissolved in water following reaction 3.

$BiVO_4$ has a flat-band potential at ∼0.2 V_{RHE},[11] and their holes are expected to locate around 2.4−2.6 V_{RHE}. Holes on the $BiVO_4$ surface have therefore enough energy to oxidize Bi(III) at 1.4−1.6 V_{RHE}, according to the Bi−H_2O Pourbaix diagram.[27] Holes prefer to participate in more cathodic reactions at the surface, including water oxidation at 1.23 V_{RHE}, or oxidation of the hole scavenging citrate, generalized as reaction 1 in Scheme 1. As a result, Bi(III) oxidation can be protected by the more cathodic reactions in the electrolyte, which renders the photoanode stable against self-oxidation.[1,32] Nevertheless, dissolution measured in the study shows the existence of self-oxidation.

Taking Bi(III) oxidation as the PEC dissolution mechanism, the dissolution current $i_{dissolution}$ can be evaluated by $i_{dissolution} = zF\dot{n}$, where z is the charge transfer of the redox reaction, F = 96485 A mol^{-1} is the Faraday constant, and $\dot{n}$ is the PEC dissolution rate of Bi. Assuming an average charge transfer of z = 1, the calculated dissolution current is compared with the photocurrent in Figure 5. From 1.6 to 0.4 V_{RHE}, the oxidation photocurrent decreases, whereas the dissolution current remains the same.

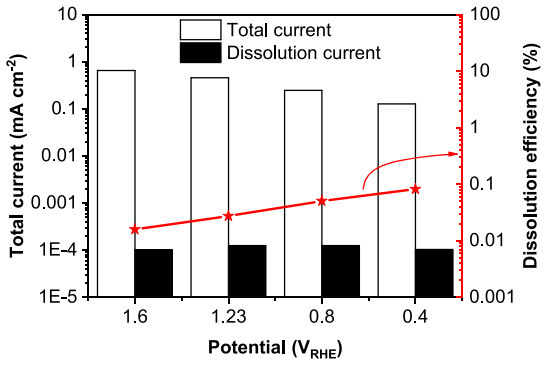

Figure 5. Comparison between the photocurrent density and the PEC dissolution current densitiy derived from Figure 3 and the Faraday efficiency of the PEC dissolution (star symbols corresponding to the right axis).

The Faraday efficiency of the dissolution process $\eta_{dissolution} = i_{dissolution}/i_{total}$ is defined by the ratio between the dissolution current and the total current i_{total} measured during light on. As shown in Figure 5, the Faraday efficiency of dissolution increases from ∼0.01% at 1.6 V_{RHE} to ∼0.1% at 0.4 V_{RHE}. In other words, $BiVO_4$ self-oxidation occurs once for 1000−

DOI: 10.1021/acs.jpcc.9b07220
J. Phys. Chem. C 2019, 123, 23410−23418

10000 of transferred holes. This is in agreement with the mechanistic picture that electrolyte oxidation is the more favorable reaction and hence limits the rates and efficiency of $BiVO_4$ self-oxidation. For OER, stability number has been introduced as a metric to benchmark the stability of electrodes against dissolution,[33] which is roughly speaking inversely proportional to the Faraday efficiency of dissolution. $BiVO_4$ is more stable under conditions when the Faraday efficiency of dissolution is lower.

Despite the seemingly low Faraday efficiency of dissolution, a photocorrosion rate of 0.05 nm min^{-1} (1.5 pmol cm^{-2} s^{-1}) suggests complete removal of a 100 nm $BiVO_4$ film in 2000 min, just over a day. A further reduction of dissolution by 2−3 orders of magnitude is necessary for applications. By introducing a protection layer on top, $BiVO_4$ surface can be insulated from the electrolyte. Water oxidation catalysts can offer very effective protection,[1,9,10,18,32] as they provide more active sites for the photogenerated holes to oxidize water, thereby further limiting the population of holes in $BiVO_4$ and hence the self-oxidation.

CONCLUSION

In summary, we have demonstrated time-resolved dissolution studies on $BiVO_4$ photoanodes that further shed light on the mechanisms of photocorrosion.

1. Time-resolved measurement reveals dissolution upon contact with the electrolyte. The amount of contact dissolution remains similar regardless of the contact potential. Chemical dissolution of V-rich oxide is a likely mechanism, and the resulting surface becomes more Bi-rich.

2. PEC dissolution of $BiVO_4$ is an order of magnitude higher than the dissolution in the dark between 0.4 and 1.6 V_{RHE}. The independence of PEC dissolution on the potential in this range suggests Bi(III) oxidation as the main mechanism of PEC dissolution. The branching ratio between Bi(III) self-oxidation and the oxidation of water and the hole scavenging citrate is 1:1000−1:10000 depending on the potential, as the latter reactions protect $BiVO_4$ from the former photocorrosion pathway. At the open circuit potential, 0.2 V_{RHE}, PEC dissolution is much lower yet still higher than the dissolution in the dark.

3. PEC dissolution rates in the 5 and 15 mM citrate electrolytes are very similar and comparable to the rates evaluated in neutral 0.1 and 1 M phosphate buffers.[17] The chelating effect of citrate electrolytes keeps the otherwise insoluble Bi ions in the electrolyte, and hence a stoichiometric dissolution rate is observed with respect to V. Near-stoichiometric Bi dissolution was also observed in phosphate electrolytes,[17] possibly due to the chelating effect of polymeric phosphate ions.

AUTHOR INFORMATION

Corresponding Authors

*E-mail: siyuan.zhang@mpie.de.
*E-mail: s.cherevko@fz-juelich.de.

ORCID

Siyuan Zhang: 0000-0001-7045-0865
Olga Kasian: 0000-0001-6315-0637
Anna Fischer: 0000-0003-4567-3009
Christina Scheu: 0000-0001-7916-1533
Serhiy Cherevko: 0000-0002-7188-4857

Notes

The authors declare no competing financial interest.

ACKNOWLEDGMENTS

We thank Professor Laurie Peter for his discussion and comments on the manuscript. This research is funded by German Research Foundation (DFG) under the special programme SPP 1613 [DFG SCHE 634/12-2, DFG FI 1885/1-2].

ADDITIONAL NOTES

[a]The Roman numeral in the parentheses refers to the oxidation state of the element.
[b]All electrode potentials referred to in this study are with respect to the reversible hydrogen electrode, RHE. The unit symbol V_{RHE} was used to avoid confusion with the abbreviation of vanadium, V.

REFERENCES

(1) Eichhorn, J.; Liu, G.; Toma, F. M. In *Integrated Solar Fuel Generators*; Sharp, I. D., Atwater, H. A., Lewerenz, H.-J., Eds.; The Royal Society of Chemistry: 2019; Chapter 8, pp 281−303.
(2) Kudo, A.; Ueda, K.; Kato, H.; Mikami, I. Photocatalytic O_2 Evolution Under Visible Light Irradiation on $BiVO_4$ in Aqueous $AgNO_3$ Solution. *Catal. Lett.* **1998**, *53*, 229−230.
(3) Sayama, K.; Nomura, A.; Zou, Z.; Abe, R.; Abe, Y.; Arakawa, H. Photoelectrochemical Decomposition of Water on Nanocrystalline $BiVO_4$ Film Electrodes Under Visible Light. *Chem. Commun.* **2003**, 2908−2909.
(4) Kudo, A.; Omori, K.; Kato, H. A Novel Aqueous Process for Preparation of Crystal Form-Controlled and Highly Crystalline $BiVO_4$ Powder from Layered Vanadates at Room Temerpature and Its Photocatalytic and Photophysical Properties. *J. Am. Chem. Soc.* **1999**, *121*, 11459−11467.
(5) Park, Y.; McDonald, K. J.; Choi, K.-S. Progress in Bismuth Vanadate Photoanodes for Use in Solar Water Oxidation. *Chem. Soc. Rev.* **2013**, *42*, 2321.
(6) Kim, J. H.; Lee, J. S. $BiVO_4$-Based Heterostructured Photocatalysts for Solar Water Splitting: A Review. *Energy Environment Focus* **2014**, *3*, 339−353.
(7) Sivula, K.; Van de Krol, R. Semiconducting Materials for Photoelectrochemical Energy Conversion. *Nat. Rev. Mater.* **2016**, *1*, 15010.
(8) Tolod, K. R.; Hernandez, S.; Russo, N. Recent Advances in the $BiVO_4$ Photocatalysts for Sun-Driven Water Oxidation: Top-Performing Photoanodes and Scale-up Challenges. *Catalysts* **2017**, *7*, 13.
(9) Garcia-Tecedor, M.; Cardenas-Morcoso, D.; Fernandez-Climent, R.; Gimenez, S. The Role of Underlayers and Overlayers in Thin Film $BiVO_4$ Photoanodes for Solar Water Splitting. *Adv. Mater. Interfaces* **2019**, *6*, 1900299.
(10) Kim, J. H.; Lee, J. S. Elaborately Modified $BiVO_4$ Photoanodes for Solar Water Splitting. *Adv. Mater.* **2019**, *31*, 1806938.
(11) Rohloff, M.; Anke, B.; Zhang, S.; Gernert, U.; Scheu, C.; Lerch, M.; Fischer, A. Mo-Doped $BiVO_4$ Thin Films − High Photoelectrochemical Water Splitting Performance Achieved by a Tailored Structure and Morphology. *Sustainable Energy Fuels* **2017**, *1*, 1830−1846.
(12) Rohloff, M.; Anke, B.; Kasian, O.; Zhang, S.; Lerch, M.; Scheu, C.; Fischer, A. Enhanced Photoelectrochemical Water Oxidation Performance by Fluorine Incorporation in $BiVO_4$ and Mo: $BiVO_4$ Thin Film Photoanodes. *ACS Appl. Mater. Interfaces* **2019**, *11*, 16430−16442.
(13) Abdi, F. F.; Firet, N.; Van de Krol, R. Efficient $BiVO_4$ Thin Film Photoanodes Modified with Cobalt Phosphate Catalyst and W-Doping. *ChemCatChem* **2013**, *5*, 490−496.
(14) Kim, J. H.; Jang, J.-W.; Jo, Y. H.; Abdi, F. F.; Lee, Y. H.; Van de Krol, R.; Lee, J. S. Hetero-type Dual Photoanodes for Unbiased Solar

DOI: 10.1021/acs.jpcc.9b07220
J. Phys. Chem. C 2019, 123, 23410−23418

Water Splitting with Extended Light Harvesting. *Nat. Commun.* **2016**, *7*, 13380.
(15) Sayama, K.; Nomura, A.; Arai, T.; Sugita, T.; Abe, R.; Yanagida, M.; Oi, T.; Iwasaki, Y.; Abe, Y.; Sugihara, H. Photoelectrochemical Decomposition of Water into H_2 and O_2 on Porous $BiVO_4$ Thin-film Electrodes Under Visible Light and Significant Effect of Ag Ion Treatment. *J. Phys. Chem. B* **2006**, *110*, 11352−11360.
(16) Berglund, S. P.; Flaherty, D. W.; Hahn, N. T.; Bard, A. J.; Mullins, C. B. Photoelectrochemical Oxidation of Water Using Nanostructured $BiVO_4$ Films. *J. Phys. Chem. C* **2011**, *115*, 3794−3802.
(17) Toma, F. M.; Cooper, J. K.; Kunzelmann, V.; McDowell, M. T.; Yu, J.; Larson, D. M.; Borys, N. J.; Abelyan, C.; Beeman, J. W.; Yu, K. M.; Yang, J.; Chen, L.; Shaner, M. R.; Spurgeon, J.; Houle, F. A.; Persson, K. A.; Sharp, I. D. Mechanistic Insights into Chemical and Photochemical Transformations of Bismuth Vanadate Photoanodes. *Nat. Commun.* **2016**, *7*, 12012.
(18) Lee, D. K.; Choi, K.-S. Enhancing Long-Term Photostability of $BiVO_4$ Photoanodes for Solar Water Splitting by Tuning Electrolyte Composition. *Nat. Energy* **2018**, *3*, 53−60.
(19) Chen, S.; Wang, L.-W. Thermodynamic Oxidation and Reduction Potentials of Photocatalytic Semiconductors in Aqueous Solution. *Chem. Mater.* **2012**, *24*, 3659−3666.
(20) Klemm, S. O.; Topalov, A. A.; Laska, C. A.; Mayrhofer, K. J. J. Coupling of a High Throughput Microelectrochemical Cell with Online Multielemental Trace Analysis by ICP-MS. *Electrochem. Commun.* **2011**, *13*, 1533−1535.
(21) Schuppert, A. K.; Topalov, A. A.; Katsounaros, I.; Klemm, S. O.; Mayrhofer, K. J. J. A Scanning Flow Cell System for Fully Automated Screening of Electrocatalyst Materials. *J. Electrochem. Soc.* **2012**, *159*, F670−F675.
(22) Knöppel, J.; Zhang, S.; Speck, F. D.; Mayrhofer, K. J. J.; Scheu, C.; Cherevko, S. Time-Resolved Analysis of Dissolution Phenomena in Photoelectrochemistry − A Case Study of WO_3 Photocorrosion. *Electrochem. Commun.* **2018**, *96*, 53−56.
(23) Kennedy, J. H.; Frese, K. W., Jr. Photooxidation of Water at α-Fe_2O_3 Electrodes. *J. Electrochem. Soc.* **1978**, *125*, 709−714.
(24) Post, K.; Robins, R. G. Thermodynamic Diagrams for the Vanadium − Water System at 298.15 K. *Electrochim. Acta* **1976**, *21*, 401−405.
(25) Povar, I.; Spinu, O.; Zinicovscaia, I.; Pintilie, B.; Ubaldini, S. Revised Pourbaix Diagrams for the Vanadium − Water System. *J. Electrochem. Sci. Eng.* **2019**, *9*, 75−84.
(26) Zhou, Z. H.; Zhang, H.; Jiang, Y.-Q.; Lin, D.-H.; Wan, H.-L.; Tsai, K.-R. Complexation Between Vanadium(V) and Citrate: Spectroscopic and Structural Characterization of a Dinuclear Vanadium(V) Complex. *Transition Met. Chem.* **1999**, *24*, 605−609.
(27) Pourbaix, M. *Atlas of Electrochemical Equilibria in Aqueous Solutions;* National Association of Corrosion Engineers: 1974.
(28) Asato, E.; Katsura, K.; Mikuriya, M.; Fujii, T.; Reedijk, J. Synthesis, Structure, and Spectroscopic Characterization of Bismuth Citrate Compounds and Bismuth-Containing Ulcer Healing Agent Colloidal Bismuth Subcitrate (CBS). 3. Crystal and Solution Structures of $K(NH_4)[Bi_2(cit)_2(H_2O)_2](H_2O)_x$ (x = 2, 4). *Inorg. Chem.* **1993**, *32*, 5322−5329.
(29) Sadler, P. J.; Sun, H. Ranitidine Bismuth (III) Citrate. *J. Chem. Soc., Dalton Trans.* **1995**, 1395−1401.
(30) Bismuth citrate − Registration Dossier − ECHA; https://echa.europa.eu/registration-dossier/-/registered-dossier/11383/4/9 (accessed Aug 23, 2019).
(31) Rashchi, F.; Finch, J. A. Polyphosphates: A Review. Their Chemistry and Application with Particular Reference to Mineral Processing. *Miner. Eng.* **2000**, *13*, 1019−1035.
(32) Bae, D.; Seger, B.; Vesborg, P. C. K.; Hansen, O.; Chorkendorff, I. Strategies for Stable Water Splitting via Protected Photoelectrodes. *Chem. Soc. Rev.* **2017**, *46*, 1933−1954.
(33) Geiger, S.; Kasian, O.; Ledendecker, M.; Pizzutilo, E.; Mingers, A. M.; Fu, W. T.; Diaz-Morales, O.; Li, Z.; Oellers, T.; Fruchter, L.; et al. The Stability Number as a Metric for Electrocatalyst Stability Benchmarking. *Nat. Catalysis* **2018**, *1*, 508−515.

DOI: 10.1021/acs.jpcc.9b07220
J. Phys. Chem. C 2019, 123, 23410−23418